Molecular Imaging of Chimeric Antigen Receptor T Cells by ICOS-ImmunoPET

Federico Simonetta[1,2,3], Israt S. Alam[4], Juliane K. Lohmeyer[1], Bita Sahaf[5], Zinaida Good[5,6,7], Weiyu Chen[4], Zunyu Xiao[4], Toshihito Hirai[1], Lukas Scheller[1], Pujan Engels[1], Ophir Vermesh[4], Elise Robinson[4], Tom Haywood[4], Ataya Sathirachinda[4], Jeanette Baker[1], Meena B. Malipatlolla[5], Liora M. Schultz[8], Jay Y. Spiegel[5], Jason T. Lee[4,5,9], David B. Miklos[1], Crystal L. Mackall[1,5,7,8], Sanjiv S. Gambhir[4,10,†], and Robert S. Negrin[1]

ABSTRACT

Purpose: Immunomonitoring of chimeric antigen receptor (CAR) T cells relies primarily on their quantification in the peripheral blood, which inadequately quantifies their biodistribution and activation status in the tissues. Noninvasive molecular imaging of CAR T cells by PET is a promising approach with the ability to provide spatial, temporal, and functional information. Reported strategies rely on the incorporation of reporter transgenes or *ex vivo* biolabeling, significantly limiting the application of CAR T-cell molecular imaging. In this study, we assessed the ability of antibody-based PET (immunoPET) to noninvasively visualize CAR T cells.

Experimental Design: After analyzing human CAR T cells *in vitro* and *ex vivo* from patient samples to identify candidate targets for immunoPET, we employed a syngeneic, orthotopic murine tumor model of lymphoma to assess the feasibility of *in vivo* tracking of CAR T cells by immunoPET using the ^{89}Zr-DFO-anti-ICOS tracer, which we have previously reported.

Results: Analysis of human CD19-CAR T cells during activation identified the Inducible T-cell COStimulator (ICOS) as a potential target for immunoPET. In a preclinical tumor model, ^{89}Zr-DFO-ICOS mAb PET-CT imaging detected significantly higher signal in specific bone marrow–containing skeletal sites of CAR T-cell–treated mice compared with controls. Importantly, administration of ICOS-targeting antibodies at tracer doses did not interfere with CAR T-cell persistence and function.

Conclusions: This study highlights the potential of ICOS-immunoPET imaging for monitoring of CAR T-cell therapy, a strategy readily applicable to both commercially available and investigational CAR T cells.

See related commentary by Volpe et al., p. 911

Introduction

Chimeric antigen receptor (CAR) T-cell therapy has shown impressive results in B-cell hematologic malignancies leading to the clinical approval of the first engineered cellular therapy for cancer (1, 2). In contrast to conventional pharmacologic approaches, CAR T cells are living drugs that after administration actively migrate to target tumor-infiltrated tissues, expand, and persist to exert their function efficiently. The development of new CAR T-cell–based therapies and the improvement of existing ones are greatly influenced by our ability to monitor their *in vivo* dynamics to gain greater insights into the success or failure of this treatment approach. The measurement of circulating CAR T cells in the peripheral blood by flow cytometry and/or PCR is the only immuno-monitoring modality currently available. Some studies have reported an association between the peak and the duration of circulating CAR T-cell levels and the clinical outcome (3–7), while other studies have failed to confirm these results (8, 9), suggesting that such a measure might not accurately reflect the actual biodistribution and persistence of the cells in the body. Such a discrepancy can be particularly relevant when CAR T cells are employed for the treatment of solid tumors for which lack of efficient migration to the tumor site is considered one of the main barriers limiting the efficacy of CAR T-cell therapy (2, 10).

Molecular imaging is an attractive strategy for noninvasive and longitudinal monitoring of CAR T-cell distribution *in vivo*. To date, several studies using PET imaging have been conducted because of the high sensitivity and quantitative capabilities of this clinically relevant imaging modality. The majority of the preclinical and clinical pilot studies published so far involve the use of reporter genes inserted into the CAR construct for the detection of CAR T cells (11–15). Despite the enormous potential of this indirect labeling approach, major limitations of this strategy are the requirement for the generation and approval of entirely new CAR T cells, specifically designed to incorporate the imaging functionality, and a significant risk of immunogenicity. To circumvent these limitations, an alternative approach that has been tested involves the *ex vivo* labeling of CAR T cells with

[1]Division of Blood and Marrow Transplantation, Department of Medicine, Stanford University, Stanford, California. [2]Division of Hematology, Department of Oncology, Geneva University Hospitals and Faculty of Medicine, University of Geneva, Geneva, Switzerland. [3]Translational Research Center for Oncohematology, Department of Internal Medicine Specialties, University of Geneva, Geneva, Switzerland. [4]Bio-X Program and Molecular Imaging Program at Stanford (MIPS), Department of Radiology, Stanford University School of Medicine, Stanford, California. [5]Stanford Cancer Institute, Stanford University, Stanford, California. [6]Department of Biomedical Data Science, Stanford University, Stanford, California. [7]Parker Institute for Cancer Immunotherapy, San Francisco, California. [8]Department of Pediatrics, Stanford University, Stanford, California. [9]Stanford Center for Innovation in *In Vivo* Imaging (SCi^3), Stanford University School of Medicine, Stanford, California. [10]Departments of Bioengineering and Materials Science & Engineering, Bio-X, Stanford University, Stanford, California.

Note: Supplementary data for this article are available at Clinical Cancer Research Online (http://clincancerres.aacrjournals.org/).

F. Simonetta and I.S. Alam contributed equally to this article.

S.S. Gambhir and R.S. Negrin contributed equally to this article.

[†]Deceased.

Corresponding Author: Robert S. Negrin, Stanford University, Stanford, CA 94305. Phone: 650-723-0822; E-mail: negrs@stanford.edu

Clin Cancer Res 2021;27:1058–68

doi: 10.1158/1078-0432.CCR-20-2770

©2020 American Association for Cancer Research.

Downloaded from http://aacrjournals.org/clincancerres/article-pdf/27/4/1058/2067888/1058.pdf by guest on 19 August 2022

Translational Relevance

Chimeric antigen receptor (CAR) T cells have revolutionised the treatment of B-cell malignancies, and there are substantial ongoing efforts to apply this powerful strategy to other forms of cancer. The development of new CAR T-cell–based therapies and the improvement of existing therapies are greatly influenced by our ability to monitor their pharmacodynamics *in vivo*. The measurement of circulating CAR T cells in the peripheral blood, which lacks vital spatial information, is so far the only immuno-monitoring modality currently available. In this work we demonstrated that immunoPET targeting Inducible T-cell COStimulator (ICOS or CD278), a costimulatory molecule upregulated during T-cell activation, enables *in vivo* imaging of activated CAR T cells at the tumor site. This molecular imaging approach targeting an endogenous biomarker does not require the addition of reporter genes or *ex vivo* labeling and is, therefore, potentially applicable to the clinical setting for the study of any commercially available and investigational CAR T-cell products.

radioactive tracers prior to administration (16–18). This approach has the advantage of being applicable to any CAR T cells, including the current commercially available ones, but has several limitations, principally limited temporal resolution, a function of the radioactive decay of the label employed. Even if radioisotopes with long half-lives are employed, imaging is limited to a relatively short time frame after administration and is further compounded by signal dilution as CAR T cells proliferate *in vivo*.

ImmunoPET is a rapidly expanding area of molecular imaging that employs mAbs and antibody fragments radiolabeled with PET isotopes, thereby combining the ultra-high specificity and affinity of antibodies for cell surface markers with the superior sensitivity of PET (19). Advantageously, the radiolabeled antibodies can be injected at different timepoints after administration of the cells and even repeatedly to allow longitudinal and serial assessment of CAR T-cell persistence. Target molecules evaluated to date to study T-cell immune responses principally include lineage defining molecules, such as CD3 (20, 21), CD4 (22, 23), CD7 (24), and/or CD8 (25, 26), and T-cell surface activation markers, such as OX40 (27), HLA-DR (28), and ICOS (29). Our group and others have evaluated such approaches for monitoring different classes of cancer immunotherapies in preclinical models, including tumor vaccination (27, 29), immune checkpoint blockade (29), and allogeneic hematopoietic stem cell transplantation (28, 30).

In this work, we identified Inducible T-cell COStimulator (ICOS or CD278), a costimulatory molecule upregulated during T-cell activation (31), as a candidate target for CAR T-cell monitoring using immunoPET. Moreover, we assessed the utility of ICOS-targeted immunoPET to monitor CD19-specific CAR T-cell activation, expansion, and homing to target tumor-infiltrated tissues in a murine model of B-cell lymphoma.

Materials and Methods

Analysis of RNA sequencing data obtained from human CAR T cells during *in vitro* activation

We analyzed an RNA sequencing (RNA-seq) dataset we recently published (32) and deposited in NCBI Gene Expression Omnibus, series accession number, GSE136891. RNA-seq data were obtained at serial timepoints from CD19.CD28z CAR T cells generated from naïve ($CD45RA^+$, $CD45RO^-$, $CD62L^+$, $CCR7^+$, $CD95^-$, and $CD122^-$) $CD4^+$ or $CD8^+$ T cells as detailed in ref. 32.

Mass cytometry analysis of human CAR T cells

We retrospectively analyzed *ex vivo* ICOS expression on human CD19-28z CAR T cells in prospectively collected data obtained from 31 patients receiving commercial axicabtagene ciloleucel at Stanford University (Stanford, CA) for relapsed or refractory diffuse large B-cell lymphoma (DLBCL). Mass cytometry analysis was performed as described previously (33). The mass cytometry panel assessed expression of 33 surface or intracellular proteins relevant to T-cell function in blood collected on day 7 (peak expansion) and on day 21 (late expansion) post–CAR T-cell infusion (33). ICOS expression was evaluated on live CAR-expressing T cells identified by anti-idiotype antibody provided by Dr. Laurence Cooper (University of Texas MD Anderson Cancer Center, Houston, TX; ref. 34). Written informed consent was provided by all patients enrolled, and the study was approved by the Stanford University Institutional Review Board (Stanford, CA). Experimental procedures were carried out in accordance with the ethical principles of the Declaration of Helsinki.

Animals

BALB/cJ mice were purchased from the Jackson Laboratory. Firefly luciferase $(Luc)^+$ transgenic BALB/c mice have been reported previously (35) and were bred in our animal facility at Stanford University (Stanford, CA). All procedures were performed on sex-matched animals between 8 and 12 weeks of age and approved by Stanford University's Administrative Panel for Laboratory Animal Care/Institutional Animal Care and Use Committee in compliance with the guidelines of humane care of laboratory animals.

Murine CAR T cells generation

CAR T cells specifically recognizing the murine CD19 (mCD19) molecule and including a CD28 costimulatory domain were generated as reported previously (36, 37). mCD19 CAR stable producer cell line (37) was kindly provided by Dr. Terry J. Fry (University of Colorado School of Medicine, Aurora, CO). T cells were enriched from BALB/c mouse spleen single-cell suspensions using the mouse Pan T Cell Isolation Kit II (Miltenyi Biotec) according to the manufacturer's protocol. T cells were activated for 24 hours with Dynabeads Mouse T-Activator CD3/CD28 (Life Technologies) in the presence of human IL2 (30 U/mL) and murine IL7 (10 ng/mL; PeproTech) in RPMI1640 media supplemented with 10% heat-inactivated FBS, 1 mmol/L sodium pyruvate, 2 mmol/L glutamine, 100 U/mL penicillin, and 100 μg/mL streptomycin at 37°C with 5% CO_2. Activated T cells were then transduced with mCD19 CAR by culturing them for 48 hours in RetroNectin-coated plates loaded with supernatant harvested from the stable producer line 48 hours after culture. Dynabeads were then removed, and after washing, cells were rested for 24 hours in fresh medium containing IL2 and IL7 before use. Transduction efficiency was measured by flow cytometry after protein L staining (38). Cell numbers were adjusted on the basis of transduction efficacy (50% on average) before *in vitro* or *in vivo* use.

In vitro cytotoxic assay

Murine CD19.28z (mCD19.28z) CAR T cells were cocultured with luciferase-transduced A20 cells ($A20^{luc}$; ref. 39) at different ratios adjusted on the basis of transduction efficiency in culture medium consisting of RPMI1640, supplemented with L-glutamine (2 mmol/L), penicillin (100 U/mL), streptomycin (0.1 mg/mL), 2-mercaptoethanol

Downloaded from http://aacrjournals.org/clincancerres/article-pdf/27/4/1058/2067888/1058.pdf by guest on 19 August 2022

(5 × 10e-5 mol/L), and 10% FBS. After 24 hours of culture, D-luciferin (PerkinElmer) was added at 5 μg/mL and incubated for 5 minutes at room temperature before imaging using an IVIS Spectrum Imaging System (PerkinElmer). For ICOS expression analysis, CAR T cells cultured with $A20^{Luc+}$ at 1:1 ratio or unstimulated controls were harvested and analyzed by flow cytometry.

In vivo murine tumor model

We employed a systemic B-cell lymphoma mouse model that we have reported previously, in which tumor cells infiltrate secondary lymphoid organs and bone marrow (BM; ref. 39). Briefly, CD19-expressing A20 cells were purchased from ATCC in 2017, expanded for three passages, and cryopreserved until use. A20 cells were thawed, cultured for maximum a week, resuspended in PBS, and injected intravenously (2.5 × 10e5 cells/mouse) by tail vein into sublethally (4.4 Gy) irradiated $Thy1.2^+$ BALB/c recipient mice. Seven days after tumor injection, Luc^+ CAR T cells (1 × 10e6 transduced cells/mouse adjusted on transduction efficiency) or equivalent numbers of *in vitro* expanded untransduced Luc^+ T cells were administered by retro-orbital intravenous injection. In tumor homing experiments, $A20^{Luc+}$ cells were employed and mice were left untreated.

Flow cytometry analysis

Single-cell suspensions were prepared from spleen and BM in PBS containing 2% FBS. Extracellular staining was preceded by incubation with purified FC Blocking Reagent (Miltenyi Biotec). Cells were stained with FITC anti-CD45.1 (clone A20), BV785 anti-ICOS (clone C398.4A) or appropriate isotype control (clone HTK888), APC anti-Thy1.1 (clone OX-7), APC/Fire750 anti-CD19 (clone 6D5), BV421 anti-CD4 (clone GK1.5), BV605 anti-CD3 (clone 17A2), and BV650 anti-CD8 (clone 53-6.7). Dead cells were excluded using Fixable Viability Dye eFluor 506 (eBioscience). All antibodies were purchased from BioLegend. Samples were acquired on a BD LSR II Flow Cytometer (BD Biosciences), and analysis was performed with FlowJo 10.5.0 Software (Tree Star).

In vivo bioluminescence imaging

For *in vivo* bioluminescence imaging (BLI), mice were injected with D-luciferin (10 mg/kg, i.p.) and anesthetized with 2% isoflurane in oxygen. Imaging was conducted using an IVIS Spectrum Imaging System (PerkinElmer) and data were analyzed with Living Image Software version 4.1 (PerkinElmer), or imaging was conducted using an Ami Imaging System (Spectral Instruments Imaging) and data were analyzed with Aura Software (Spectral Instruments Imaging).

Bioconjugation and radiolabeling of ICOS-targeted mAb

ICOS-targeted mAb (ICOS mAb, clone:7E.17G9, BioXCell) was modified with the bifunctional chelator, deferoxamine (DFO/p-SCN-Bn-Deferoxamine, Macrocyclics). Briefly, unconjugated mAb was prepared at 1 mg/mL in PBS (pH = 7.4), and buffer exchanged with PBS solution adjusted to pH 8.8–9.0 using 1 mol/L Na_2CO_3. Following this, 10-fold molar excess DFO was added to the ICOS mAb solution and the conjugation was allowed to proceed for 1-hour at 37°C. The mixture was subsequently thoroughly buffer exchanged using PBS (pH = 7.4) to remove unreacted DFO using a 2 mL vivaspin centrifugal concentrator with a 50K cutoff (Sartorius). The concentration of the final DFO-ICOS mAb conjugate was determined by Thermo Scientific NanoDrop One Microvolume UV-Vis Spectrophotometer.

For ^{89}Zr labeling, 37 MBq (~1 mCi) of ^{89}Zr-oxalate (3D imaging) was diluted in 0.5 mL of HEPES buffer (0.5 mol/L) to ensure a pH range of 7.0–7.5 followed by the addition of approximately 166 μg of DFO-ICOS mAb. Radiolabeling was carried out for 1 hour at 37°C with shaking, after which the radiolabeled antibody, ^{89}Zr-DFO-ICOS mAb, was purified using a 7K MW cut-off Zeba Spin Desalting Column (Thermo Fisher Scientific) centrifuged for 1 minute at 1,000 × *g*. The radiochemical yield and purity were determined via instant TLC (iTLC). Samples (2 μL) of the radiolabeling reaction and purified radiolabeled antibody were spotted into silica-impregnated radio iTLC plates, run with 50 mmol/L EDTA (pH = 4.5), and developed in a Phosphor-plate Reader (PerkinElmer). Radiolabeled antibody remained at the origin ($R_f = 0$), while free ^{89}Zr moved with the solvent front ($R_f = 1$). A final radiochemical purity of 99% was achieved, along with a final specific activity of 6 μCi/μg. The final formulation was prepared in PBS.

Small-animal PET/CT and *ex vivo* biodistribution studies

Mice were anesthetized using isoflurane (2%–2.5% for induction and 1.5%–2% for maintenance) delivered by 100% oxygen. ^{89}Zr-DFO-ICOS mAb (45 μCi ± 3.6 μCi, 7.5 μg ± 0.6 μg) was administered intravenously in untreated and Luc^+ untransduced T-cell or CAR T-cell–treated A20 tumor–bearing mice. Radiotracer administration corresponded to day 5 post–CAR T-cell injection. At 24 and 48 hours after ^{89}Zr-DFO-ICOS mAb tracer administration, mice underwent imaging with static 20-minute PET scans followed by 10-minute transmission scans for PET attenuation correction on the Inveon Dedicated PET Scanner (DPET, Siemens), and CT scans on the GNEXT (Sofie Biosciences) for anatomic coregistration of the PET data. PET image reconstruction and image analysis were conducted as described previously (27).

Following the completion of the scans 48 hours after injection of the tracer, mice were euthanized and *ex vivo* biodistribution studies were performed to measure tissue-specific radioactivity, and further corroborate PET findings. Briefly, we collected blood (~100 μL) via cardiac puncture, as well as the following tissues: heart, spleen, kidney, liver, muscle, femur, tibia, iliac bone, and lumbar spine. Harvested hearts were rinsed in clean water after an incision was made to remove residual blood, and then gently dabbed to remove excess moisture. Tissues were placed in a tube, weighed, and radioactivity was measured using an Automated Gamma Counter (Hidex AMG Automatic Gamma Counter). Tissue-associated radioactivity was normalized to tissue weight and amount of radioactivity administered to each mouse, and decay-corrected to the time of radiotracer injection. Data were expressed as percentage of injected dose per gram of tissue (%ID/g) values.

Assessment of the impact of ICOS mAb administration at imaging doses on CAR T-cell homeostasis and function

Murine-specific ICOS mAb (clone 7E.17G9; BioXCell) or isotype control (clone LTF-2; BioXCell) was administered intravenously as a single dose on day 5 after CAR T-cell administration (10 μg in 100 μL of PBS). The dose was determined on the basis of the upper limit of antibody administered during PET imaging studies.

Statistical analysis

Student two-tailed *t* test, the Mann–Whitney U test, or the Wilcoxon signed-rank test was used as appropriate to determine statistical significance. BLI data (photons/seconds) are displayed as mean and SD for each group over time and were analyzed by two-way ANOVA with Bonferroni correction. Survival curves were represented with the Kaplan–Meier method and compared by log-rank test. Statistical analyses were performed using Prism 8

Downloaded from http://aacrjournals.org/clincancerres/article-pdf/27/4/1058/2067888/1058.pdf by guest on 19 August 2022

(GraphPad Software) and R version 3.5.1 (Comprehensive R Archive Network project (http://cran.us.r-project.org) with R studio version 1.1.453.

Results

ICOS expression is upregulated and sustained during *in vitro* and *in vivo* activation of human CD19.28z CAR T cells

In an effort to identify surface activation markers as candidate targets for immunoPET, we analyzed recently published RNA sequencing data obtained from human $CD4^+$ and $CD8^+$ CD19.28z CAR T cells cultured *in vitro* (32). The analysis was restricted to a selected list of markers known to be upregulated during activation on the T-cell surface and previously employed as targets for PET imaging (27, 29, 40, 41). As shown in **Fig. 1A**, transcripts of most of the selected markers were expressed at high levels early after activation (day 7) and decreased at later timepoints (days 10 and 14). ICOS transcription exhibited a different trend, progressively increasing and being sustained at later timepoints in both $CD4^+$ and $CD8^+$ CAR T cells (**Fig. 1A**). To further validate ICOS as a candidate target for immunoPET, we next assessed its *ex vivo* expression on CD19.28z CAR T cells isolated from 31 patients receiving commercial axicabtagene ciloleucel (KTE-C19) for relapsed/refractory B-cell lymphoma, at days 7 and 21 after therapy administration. CAR-expressing T cells identified using specific anti-idiotype staining were compared with circulating T cells not expressing the CAR. ICOS was expressed at significantly higher levels on CAR-expressing (CAR^+) T cells compared with CAR-nonexpressing (CAR^-) T cells (**Fig. 1B**). This difference was observed at day 7, corresponding to the peak of CAR T-cell expansion (median intensity ± SEM: CAR^+, 26.6 ± 4.7 and CAR^-, 9.6 ± 0.9; $P = 0.00002$), and further maintained at day 21 (CAR^+, 16.3 ± 3.2 and CAR^-, 9.9 ± 1.0; $P = 0.00026$; **Fig. 1C**). In accordance with the RNA-seq data (**Fig. 1A**), we detected higher ICOS expression on both $CD4^+$ and $CD8^+$ CAR T cells (Supplementary Fig. S1). Collectively, these results identify ICOS as a promising target for CAR T-cell monitoring by immunoPET.

ICOS is upregulated during *in vitro* and *in vivo* activation of mCD19.28z CAR T cells

To test the utility of ICOS-immunoPET for *in vivo* monitoring of CAR T cells in a preclinical mouse model, we went on to assess ICOS expression during mCD19.28z CAR T-cell activation. First, we analyzed ICOS expression during a 24-hour cytotoxic assay incubating mCD19.28z CAR T cells together with the Luc^+ CD19-expressing murine B-cell lymphoma cell line A20. As expected, mCD19.28z CAR T cells exerted a dose-dependent cytotoxic effect against A20 cells

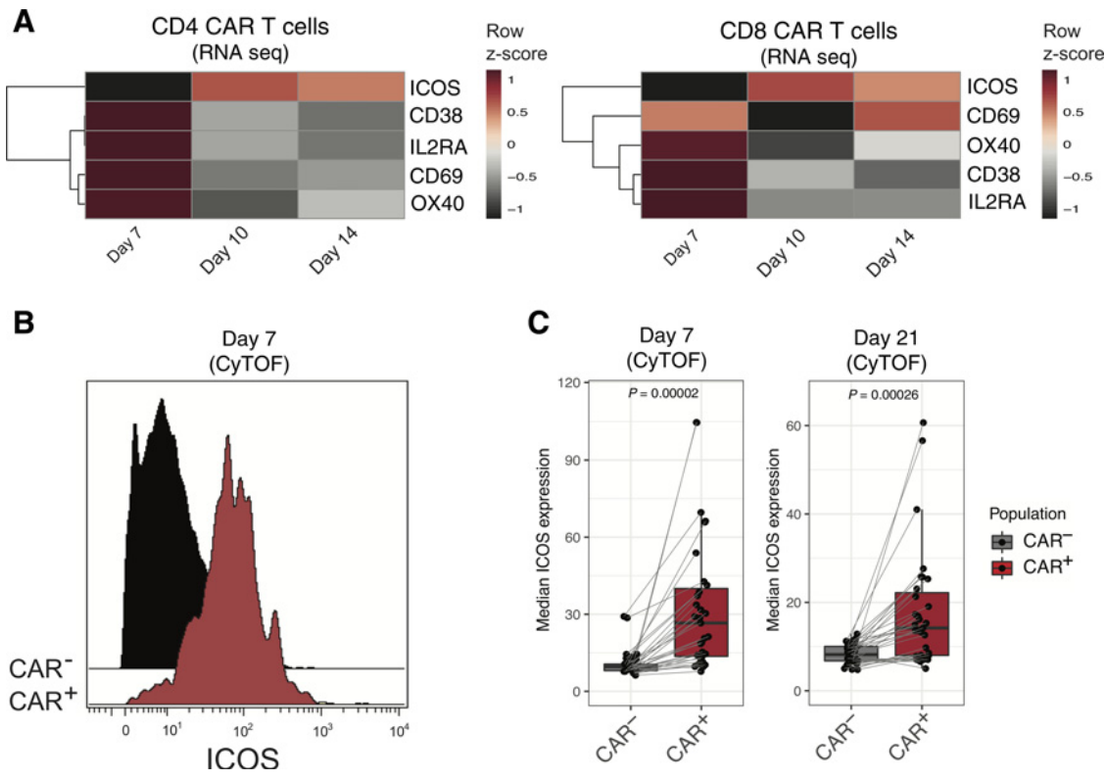

Figure 1.

ICOS is upregulated on human CD19.28z CAR T cells *in vitro* and *in vivo*. **A,** Row scaled heatmap visualization of RNA expression of the surface activation markers CD38, CD69, IL2RA, OX40, and ICOS in $CD4^+$ (left) and $CD8^+$ (right) CAR T cells on days 7, 10, and 14 of *in vitro* culture. **B,** Representative mass cytometry histogram showing ICOS expression at the surface of CAR^+ (red filled histogram) and CAR^- (black filled histogram) T cells recovered at day 7 from the peripheral blood of a patient with DLBCL receiving axicabtagene ciloleucel. **C,** Median intensity of expression of ICOS on CAR^+ (red filled boxplot) and CAR^- (gray filled boxplot) T cells recovered at day 7 (left) and day 21 (right) from the peripheral blood of patients with DLBCL ($n = 31$) receiving axicabtagene ciloleucel. Boxes represent first and third quartiles with median indicated by a line. ICOS expression on CAR^+ and CAR^- T cells was compared with the Wilcoxon signed-rank test for paired samples and *P* values are indicated.

Downloaded from http://aacrjournals.org/clincancerres/article-pdf/27/4/1058/2067888/1058.pdf by guest on 19 August 2022

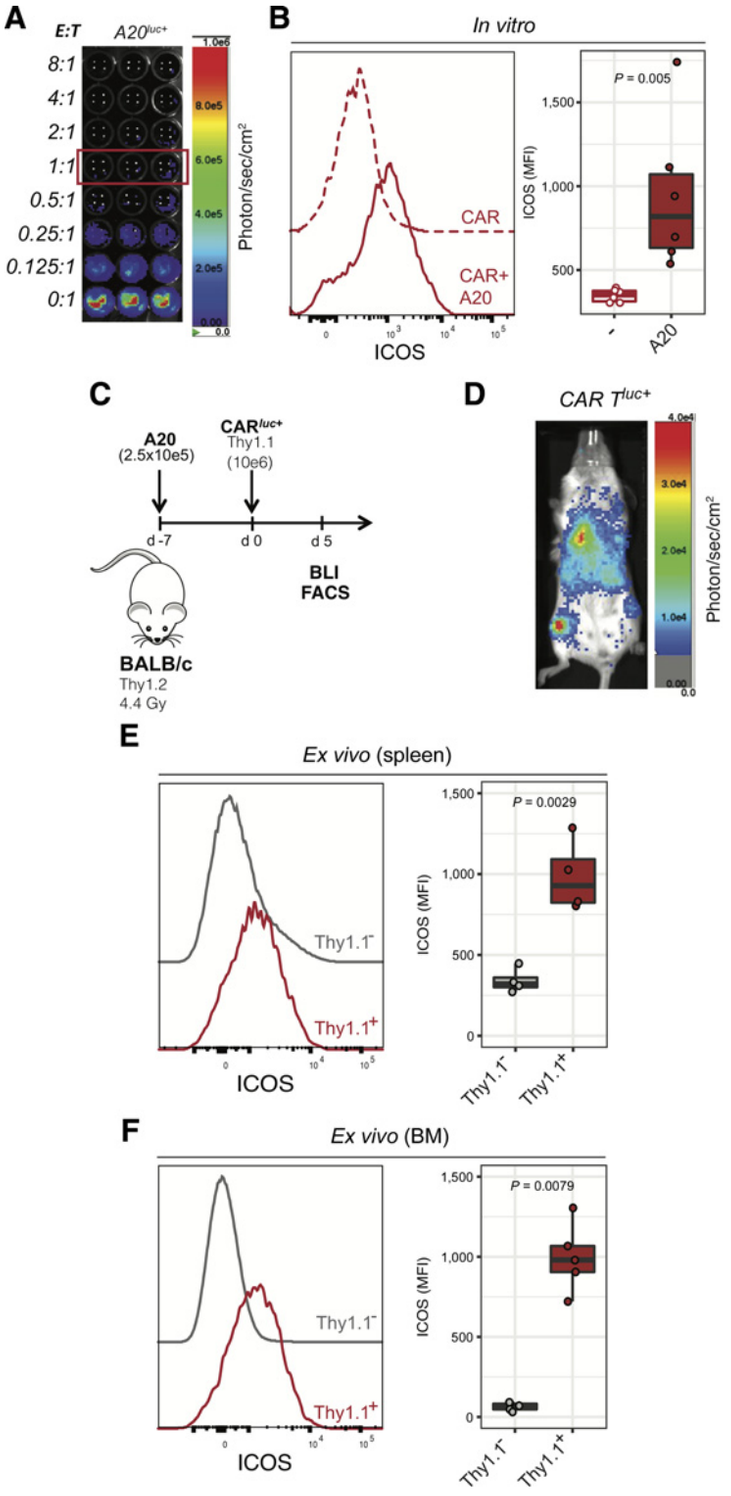

Figure 2.

ICOS is selectively expressed on activated mCD19.28z CAR T cells *in vitro* and *in vivo*. **A,** Representative *in vitro* BLI of *in vitro* cytotoxic activity of mCD19.28z CAR T cells cocultured for 24 hours with A20^{Luc+} cells at the indicated ratios of effector: target (E:T). **B,** ICOS expression on mCD19.28z CAR T cells cultured for 24 hours in the presence (solid red line and red filled box) or in the absence (dashed red line and empty box) of A20^{Luc+} cells (E:T = 1:1). Data were pooled from two independent experiments performed in triplicate. **C,** Schematic representation of the *in vivo* lymphoma tumor model employed as detailed in the text. **D,** Representative *in vivo* BLI of the biodistribution of *Luc*$^{+}$ mCD19.28z CAR T cells in the lymphoma model at day 5 after intravenous injection. Data are representative of more than five independent experiments, using a minimum of 3 mice per experiment. **E** and **F,** ICOS expression on adoptively transferred Thy1.1^{+} cells (red lines and boxes) compared with Thy1.1^{-} cells (gray lines and boxes) recovered from the spleen (**E**) or BM (**F**) at day 5 after mCD19.28z CAR T-cell injection.

(**Fig. 2A**). ICOS expression, as assessed by flow cytometry, was significantly upregulated on murine CAR T cells exposed to A20 target cells (1:1 CAR to target ratio) compared with CAR T cells alone (**Fig. 2B**). We next assessed ICOS expression on mCD19.28z CAR T cells activated *in vivo*. To better mimic the clinical scenario, we employed a systemic tumor model in which A20 lymphoma cells were injected intravenously (**Fig. 2C**). In agreement with what we have reported previously (39), by the time of CAR T-cell administration, 7 days after tumor inoculation, A20^{Luc+} cells were infiltrating the liver, the lymphoid organs, and the BM (Supplementary Fig. S2). Flow

Downloaded from http://aacrjournals.org/clincancerres/article-pdf/27/4/1058/2067888/1058.pdf by guest on 19 August 2022

cytometry analysis was performed at day 5 after administration of Thy1.1$^+$ CAR T cells into Thy1.2$^+$ recipients, a timepoint when CAR T cells had expanded and were detectable within the spleen and the BM, as confirmed by *in vivo* bioluminescence (**Fig. 2D**). ICOS expression was significantly higher at the surface of administered Thy1.1$^+$ infused cells when compared with endogenous Thy1.1$^-$ cells both in the spleen (**Fig. 2E**) and in the BM (**Fig. 2F**). To further assess the specificity of ICOS upregulation for CAR-mediated activation of CAR T cells and distinguish it from activation resulting from the lymphopenic context, we used *ex vivo* expanded untransduced T cells as an additional control. As shown in Supplementary Fig. S2B and S2C, lower percentages and absolute numbers of untransduced T cells were detected within the BM, suggesting preferential homing and/or expansion of CAR T cells in the tumor-infiltrated BM. Phenotypically, BM-infiltrating CAR T cells expressed significantly higher levels of ICOS compared with untransduced T cells (Supplementary Fig. S2C), confirming the specificity of ICOS expression for activated CAR T cells. Collectively, these results confirm that ICOS is specifically expressed on murine CAR T-cell surface during *ex vivo* and *in vivo* activation, supporting its potential utility as a biomarker for CAR T monitoring by immunoPET.

ICOS-immunoPET enables visualization of activated CAR T cells in the BM

We next tested the ability of ICOS-targeted immunoPET to visualize CAR T-cell migration, activation, and expansion during an antitumor response *in vivo* using ^{89}Zr-DFO-ICOS mAb. Employing the aforementioned murine tumor model, ^{89}Zr-DFO-ICOS mAb was intravenously injected at day 5 after T-cell administration and PET/CT images were acquired at 24 and 48 hours after tracer injection. The 48-hour timepoint was selected as the one providing superior signal-to-noise ratio. **Figure 3A** and **B** show representative volume-rendered technique (VRT) PET/CT images of tumor-bearing mice that either received no treatment (not

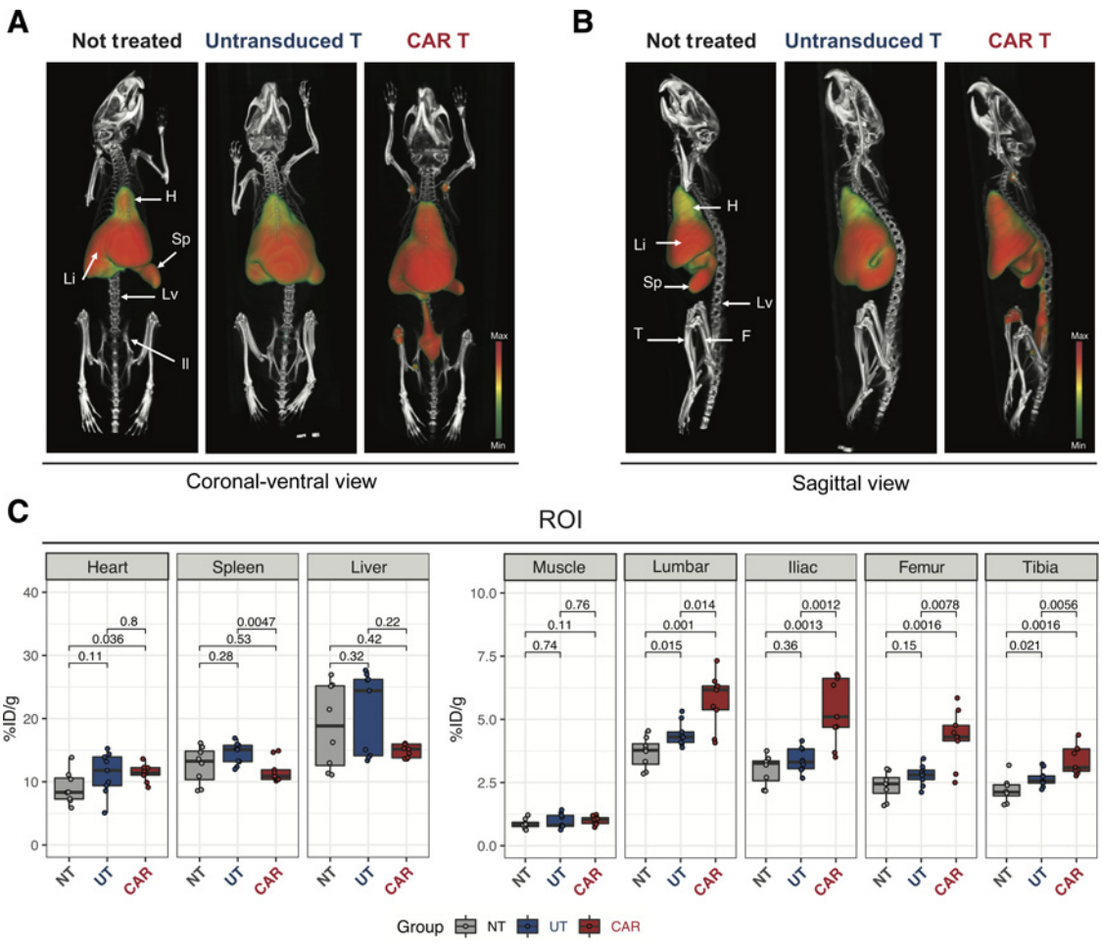

Figure 3.
^{89}Zr-DFO-ICOS mAb PET/CT imaging visualizes mCD19.28z CAR T cells during antitumor responses. **A** and **B,** Representative 3D VRT PET/CT images acquired 48 hours after tracer administration on day 5 after intravenous administration of untransduced T cells or mCD19.278z CAR T cells. Coronal-ventral views (**A**) and sagittal views (**B**) are depicted. Location of key clearance and target tissues is indicated (H, heart; Li, liver; S, spleen; Lv, lumbar vertebrae; Il, iliac bone; F, femur; and T, tibia). Images are representative of two independent experiments with 8–9 mice per group. **C,** Quantitative ROI PET image analysis of heart, spleen, liver, muscle, lumbar spine, iliac bone, femur, and tibia in mCD19.278z CAR T-cell–treated (CAR, red filled boxes), untransduced T-cell–treated (UT, blue filled boxes), and untreated controls (NT, gray filled boxes). Tracer uptake in CAR T ($n = 9$), untransduced T cell ($n = 9$), and not treated ($n = 8$) groups was compared using the Mann–Whitney U test.

Downloaded from http://aacrjournals.org/clincancerres/article-pdf/27/4/1058/2067888/1058.pdf by guest on 19 August 2022

treated, left), untransduced T cells (middle), or mCD19.28z CAR T cells (CAR T, right). PET/CT images of untreated mice showed that ^{89}Zr-DFO-ICOS mAb primarily accumulated in the heart, spleen, and liver, but not in bones, consistent with the biodistribution and clearance of intact antibodies (**Fig. 3A** and **B**, left; Supplementary Fig. S3). Mice receiving untransduced T cells, as well as CAR T cells, displayed a tracer biodistribution in highly vascularized organs (heart, liver, and spleen) similar to mice that were not treated. Importantly, we detected significantly higher ^{89}Zr-DFO-ICOS mAb PET signals in the bones of CAR T-cell–treated mice compared with both untreated mice and mice treated with untransduced T cells [**Fig. 3A** and **B**, right; two-dimensional maximum intensity projection (MIP) images in Supplementary Fig. S3]. The PET signal in the CAR T-cell–treated mice was particularly prominent in the lumbar spine, iliac bones, femur, tibia, and humeral heads (**Fig. 3A** and B, right; MIP images in Supplementary Fig. S3).

To quantify radiotracer accumulation in specific tissues and corroborate the trends observed in the PET images, we conducted a region of interest (ROI) analysis on multiple tissues guided by CT. We detected a slight, but statistically significant increase in radiotracer accumulation in the heart of CAR T-cell–treated mice compared with mice that were not treated (mean ± SEM, 11.4 ± 0.45 %ID/g vs. 9.1 ± 0.9 %ID/g; $P < 0.05$; **Fig. 3C**), while no significant differences were detected when compared with mice receiving untransduced T cells (**Fig. 3C**). No significant differences between CAR T-cell–treated mice and untreated mice were detected in spleen and liver (**Fig. 3C**). ROI quantification of PET/CT images confirmed markedly increased radiotracer uptake in bones rich in BM from CAR T-cell–treated mice compared with those of both untreated mice (lumbar vertebrae, $P = 0.001$; iliac bones, $P = 0.0013$; femur, $P = 0.0016$; and tibia, $P = 0.0016$; $n = 8$–9 per group; **Fig. 3C**) and mice receiving untransduced T cells (lumbar spine vertebrae, $P = 0.014$; iliac bones, $P = 0.0012$; femur, $P = 0.0078$; and tibia, $P = 0.0056$; $n = 9$ per group; **Fig. 3C**). As expected, there was no significant signal difference in the muscle, considered background, among the groups (**Fig. 3C**).

To corroborate the PET results, we performed a biodistribution analysis (BioD) using *ex vivo* gamma counting of the different tissues following the 48 hours PET/CT acquisition. BioD analysis confirmed higher radiotracer levels in the heart of CAR T-cell recipients compared with untreated mice ($P = 0.026$), but not with mice receiving untransduced T cells (**Fig. 4**). No difference among the groups was detected in blood, liver, and kidney (**Fig. 4**). In corroboration with the higher ICOS levels detected by FACS, BioD analysis revealed significantly higher tracer uptake in spleens from CAR T-cell–treated mice compared with the untreated group ($P = 0.0033$) and the untransduced T-cell group ($P = 0.024$; **Fig. 4**). When analyzing the bones rich in BM, we confirmed significantly higher tracer uptake in bones from

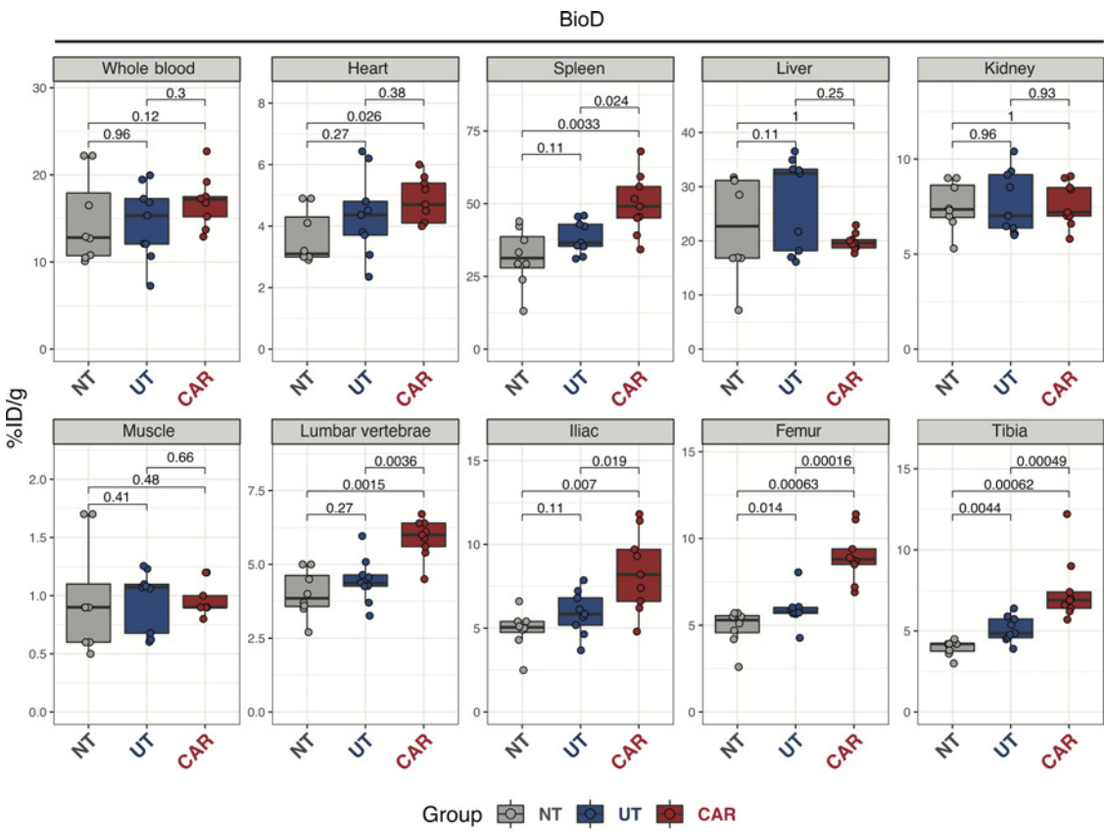

Figure 4.
Quantitative ^{89}Zr-DFO-ICOS mAb tracer biodistribution during antitumor responses. Quantification of ICOS-immunoPET signal (%ID/g) from *ex vivo* BioD analysis of whole blood, heart, spleen, liver, kidney, muscle, lumbar spine, iliac bone, femur, and tibia 48 hours after tracer administration (on day 5 after CAR T-cell therapy). Tracer uptake in CAR T-cell–treated ($n = 9$), untransduced T-cell ($n = 9$), and untreated (NT, $n = 8$) groups were compared using the Mann–Whitney U test. Results are pooled from two independent experiments with a total of 8–9 mice per group.

Downloaded from http://aacrjournals.org/clincancerres/article-pdf/27/4/1058/2067888/1058.pdf by guest on 19 August 2022

CAR T-cell–treated mice compared with mice not treated (lumbar vertebrae, $P = 0.0015$; iliac bones, $P = 0.007$; femur, $P = 0.00063$; and tibia, $P = 0.00062$) or treated with untransduced T cells (lumbar spine vertebrae, $P = 0.0036$; iliac bones, $P = 0.019$; femur, $P = 0.00016$; and tibia, $P = 0.00049$; **Fig. 4**). No difference was observed in muscle. Collectively, these results demonstrate the ability to specifically track the presence of CAR T cells at target tissues during antitumor responses *in vivo* using ^{89}Zr-DFO-ICOS mAb immunoPET.

Administration of ICOS mAb at tracer doses does not impact the *in vivo* persistence and antitumor effect of mCD19.28z CAR T cells

The use of costimulatory molecules as a target for immunoPET bears the theoretical risk of impacting CAR T-cell expansion, persistence, and ultimately *in vivo* antitumor activity, especially considering that the clone we employed (7E.17G9) blocks the interaction between ICOS and its ligand, ICOSL. To assess the impact of the administration of anti-ICOS mAbs on CAR T-cell homeostasis and function, we injected doses comparable with the maximum PET dose of anti-ICOS (clone 7E.17G9) or of the appropriate isotype control, at day 5 after CAR T-cell administration. The BLI signals derived from expanding *Luc*$^+$ CAR T cells were not significantly different between the anti-ICOS (**Fig. 5A**, top) and the isotype control groups (**Fig. 5A**, bottom and **B**). Similarly, the contraction curve of CAR T cells at later timepoints (days 10–14) did not differ in mice treated with anti-ICOS compared with mice receiving isotype control (**Fig. 5A** and **B**). Using overall survival as a measure of CAR T-cell efficacy, we did not observe any significant impact of anti-ICOS administration on the survival of untreated and CAR T-cell–treated mice when compared with mice receiving isotype control (**Fig. 5C**). Collectively, these results indicate that the administration of anti-ICOS mAb at tracer doses does not affect CAR T-cell homeostasis or antitumor activity.

Discussion

In this study, we identified ICOS-immunoPET as a promising strategy to noninvasively monitor CAR T cells *in vivo* during an antitumor response.

In vivo monitoring of CAR T-cell therapy using molecular imaging is an area of intensive investigation. Several groups, including ours, have explored the utility of reporter genes (11–15) or *ex vivo* radiolabeling approaches (16–18) to allow tracking of CAR T-cell therapies with PET. The use of immunoPET has several advantages over these approaches. First, this strategy can be applied to any CAR T-cell product, bypassing the need to insert a dedicated imaging reporter gene. The feasibility of this approach is a significant advantage considering the time and efforts required for approval of new cellular products. Second, the administration of radiolabeled antibodies at different timepoints after CAR T-cell administration, allows for serial imaging of CAR T-cell dynamics *in vivo*. This latter aspect might be essential in the clinical setting, where detection of CAR T-cell presence and activation by immunoPET might be employed to guide therapeutic decisions.

A major challenge in immunoPET imaging of adoptively transferred cells comes from the difficulties in identifying appropriate candidate targets. An ideal target should be selectively expressed on the transferred population with minimal expression on endogenous cells. In this regard, targeting surface activation markers (27–29) displays a major advantage over targeting lineage-defining markers (20–26). In this article, using an unbiased approach, we first identified

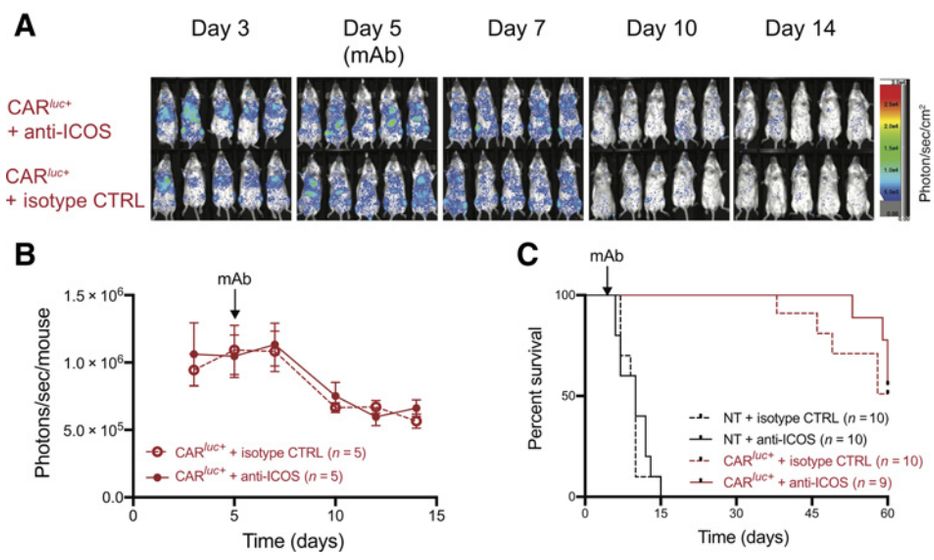

Figure 5.

Impact of anti-ICOS mAb administered at tracer dose on *in vivo* persistence and antitumor activity of mCD19.28z CAR T cells. **A** and **B,** Expansion of *Luc*$^+$ mCD19.28z CAR T cells in tumor-bearing mice treated on day 5 post-initiation of therapy, with ICOS mAb (**A**, top; **B**, continuous lines) or appropriate isotype control (**A**, bottom; **B**, dashed lines), administered at a dose similar to that employed for PET/CT studies (10 μg/mouse, representing upper limit of tracer dose). Data shown are from one experiment representative of two independent experiments with 4–5 mice per group in each experiment. **C,** Overall survival of mCD19.28z CAR T-cell–treated (CAR, red lines) or not treated (NT, black lines) mice. At day 5, mice were randomized to receive intravenous administration of ICOS mAb (continuous lines) or appropriate isotype control (dashed lines) at a dose similar to the ones employed for PET/CT studies (10 μg/mouse, representing the upper limit of tracer dose). Results are pooled from two independent experiments with a total of 9–10 mice per group. Survival curves were plotted using the Kaplan–Meier method and compared by log-rank test.

Downloaded from http://aacrjournals.org/clincancerres/article-pdf/27/4/1058/2067888/1058.pdf by guest on 19 August 2022

ICOS as a potential immunoPET target on human CAR T cells before transitioning to a murine model for the preclinical assessment of our strategy. Notably, ICOS-immunoPET enabled *in vivo* tracking of murine CAR T cells injected into immunocompetent mice bearing systemic tumors. We believe that such a model more accurately reflects the clinical scenario compared with widely employed xenogeneic tumor models, in which human CAR T cells are injected into genetically lymphopenic mice. First, it allows the evaluation of the tracer in the presence of an endogenous resident population of T cells. Second, in xenogeneic models, the injected cells are the only targets of antibodies recognizing human molecules in a murine system thus, artificially reducing the background noise coming from the endogenous population.

Another critical aspect that needs to be taken into account when developing new immuno-imaging approaches is the risk of interfering with CAR T-cell biology. The addition of reporter genes encoding foreign proteins carries a significant risk of immunogenicity (42) that can potentially limit the therapeutic potential of the CAR T cells, a risk that cannot efficiently be evaluated in preclinical xenogeneic mouse models. Moreover, the addition of extra genes to the construct might significantly interfere with CAR expression and/or function. In the case of immunoPET, antibodies may exert biological effects after ligation of their target and, depending on the blocking, agonist, or antagonist nature of the clone employed, they might interfere with CAR T-cell homeostasis and function. In our animal model, we show that the administration of tracer doses of a blocking anti-ICOS does not interfere with CAR T-cell persistence and antitumor effect, suggesting the safety of our approach. Although we cannot exclude any minor transient effects, overall there was no detectable impact on CAR T-cell expansion (as measured by BLI) or function (as assessed by the outcome analysis). Such results will need to be confirmed on human CAR T cells during clinical translation using a fully human/humanized version of the ICOS mAb.

Our study demonstrated the feasibility of utilizing immunoPET with anti-ICOS to track CAR T-cell migration into tumor-bearing mice. The early timepoint studied demonstrates the ability of the CAR T cells to migrate to their target tissue, the BM bearing the CAR-targeted CD19 antigen on infiltrating B-cell lymphoma cells, as well as on endogenous B-cell precursors. This approach is directly applicable to the clinic, yet has several limitations. First, ICOS-immunoPET was affected by a substantial nonspecific background coming from highly vascularized organs containing high amounts of blood such as heart, liver, and spleen. Such background limited the sensitivity of the assays in tumor-containing organs such as the spleen, where a significant difference between CAR T-cell–treated mice and untreated mice was detectable only in *ex vivo* biodistribution studies, but not by *in vivo* PET imaging. Such limitation could be circumvented by the use of alternative vector formats that are smaller in size and exhibit rapid pharmacokinetics and are more suitable for imaging, for example, antibody fragments, including minibodies, diabodies, single-chain variable region fragments, and nanobodies, or engineered protein scaffolds (reviewed in refs. 43, 44). Second, the intensity of ICOS expression on human CAR T cells was highly heterogeneous (**Fig. 1C**), suggesting that the CAR T-cell activation status and, therefore, the sensitivity of our approach might vary between individuals. Such heterogeneity might actually confer additional power to the ICOS-immunoPET strategy, allowing the stratification of patients based on a signal resulting from both CAR T-cell expansion and *in vivo* activation. Moreover, our analysis of human CAR T-cell phenotype was only performed on circulating CAR T cells recovered from the peripheral blood and might not reflect ICOS expression on CAR T cells at the tumor site. This may be a critical factor especially for CAR T-cell imaging in solid tumors, where the tumor microenvironment might interfere with cell activation. Finally, our preclinical study was not designed to assess the predictive potential of CAR T-cell monitoring by ICOS-immunoPET on animal survival given the high rates of tumor control in our mouse tumor model and the fact that all mice received the exact same number of CAR T cells. Clinical studies would be more appropriate to assess the relationship of site-specific tracer uptake with patient outcomes.

In conclusion, we describe for the first time, *in vivo* monitoring of CAR T-cell dynamics using immunoPET targeting an endogenous biomarker, a molecular imaging approach that does not require the addition of reporter genes or *ex vivo* labeling and that is, therefore, potentially applicable to the clinical setting for the study of any commercially available and investigational CAR T-cell products.

Authors' Disclosures

F. Simonetta reports grants from American Society for Blood and Marrow Transplantation, Geneva University Hospitals Fellowship, Swiss Cancer League, Fondation de Bienfaisance Valeria Rossi di Montelera, and Dubois-Ferrière-Dinu-Lipatti Foundation during the conduct of the study. Z. Good reports grants from Parker Institute for Cancer Immunotherapy and Stanford Cancer Institute during the conduct of the study, and personal fees from Mubadala Ventures outside the submitted work. D.B. Miklos reports grants from NCI (P01 CA049605, R.S. Negrin, principal investigator) and personal fees and nonfinancial support from Kite-Gilead during the conduct of the study. C.L. Mackall reports grants from NIH during the conduct of the study. C.L. Mackall also reports grants from Bluebird and Obsidian, as well as personal fees from Lyell Immunopharma, Nektar, Neoimmune Tech, Apricity Bio, Roche, BryoLogyx, Unum, Vor, and PACT outside the submitted work; Dr. Mackall also has numerous patents related to CAR T cells pending, issued, and licensed and a patent for CD22-CAR pending, issued, licensed, and with royalties paid from Opus/Juno/Celgene. S.S. Gambhir reports grants from Ben & Catherine Ivy Foundation, Canary Foundation, NIH, and Parker Institute for Cancer Immunotherapy during the conduct of the study. R.S. Negrin reports grants from NIH and Parker Institute for Cancer Immunotherapy during the conduct of the study. No disclosures were reported by the other authors.

Authors' Contributions

F. Simonetta: Conceptualization, data curation, formal analysis, investigation, visualization, methodology, writing-original draft. **I.S. Alam:** Conceptualization, data curation, formal analysis, investigation, visualization, methodology, writing-original draft. **J.K. Lohmeyer:** Investigation, methodology, writing-review and editing. **B. Sahaf:** Resources, data curation, investigation, methodology. **Z. Good:** Data curation, software, formal analysis, visualization, methodology. **W. Chen:** Investigation, methodology. **Z. Xiao:** Investigation, methodology. **T. Hirai:** Investigation, methodology, writing-review and editing. **L. Scheller:** Investigation, methodology. **P. Engels:** Investigation, methodology. **O. Vermesh:** Formal analysis, visualization, writing-review and editing. **E. Robinson:** Investigation, methodology. **T. Haywood:** Investigation, methodology. **A. Sathirachinda:** Investigation, methodology. **J. Baker:** Investigation, methodology. **M.B. Malipatlolla:** Investigation, methodology. **L.M. Schultz:** Investigation, methodology. **J.Y. Spiegel:** Data curation, investigation. **J.T. Lee:** Data curation, software, methodology, writing-review and editing. **D.B. Miklos:** Resources, funding acquisition, methodology. **C.L. Mackall:** Resources, supervision, funding acquisition, methodology, writing-review and editing. **S.S. Gambhir:** Conceptualization, resources, supervision, funding acquisition, project administration, writing-review and editing. **R.S. Negrin:** Conceptualization, resources, supervision, funding acquisition, project administration, writing-review and editing.

Acknowledgments

The authors would like to acknowledge the Stanford Center for Innovation in *In-Vivo* Imaging (SCi^3) and in particular, Dr. Frezghi Habte for supporting the preclinical imaging experiments. We are grateful to Rowaid Kellow and Drs. Bin Shen, Gayatri Gowrishankar, and Surya Murty for supporting radiochemistry and *in vivo* imaging studies. We also thank the Stanford shared FACS facility for their support. We would like to dedicate this work to the memory and legacy of

Downloaded from http://aacrjournals.org/clincancerres/article-pdf/27/4/1058/2067888/1058.pdf by guest on 19 August 2022

Professor S.S. Gambhir. This work was supported, in part, by funding from the Ben & Catherine Ivy Foundation (to S.S. Gambhir), the Canary Foundation (to S.S. Gambhir), NCI R01 1 CA201719-02 (to S.S. Gambhir), R01 CA23158201 (to R.S. Negrin), P01 CA49605 (to S.S. Gambhir and R.S. Negrin), P5P30CA124435 (to C.L. Mackall), the Parker Institute for Cancer Immunotherapy (to S.S. Gambhir, R.S. Negrin, C.L. Mackall, and Z. Good), the Geneva University Hospitals Fellowship (to F. Simonetta), the Swiss Cancer League (BIL KLS 3806-02-2016 to F. Simonetta), the Fondation de Bienfaisance Valeria Rossi di Montelera (Eugenio Litta Fellowship to F. Simonetta), the American Society for Blood and Marrow Transplantation (New Investigator Award 2018 to F. Simonetta), the Dubois-Ferrière-Dinu-Lipatti Foundation (to F. Simonetta), the Virginia and D.K. Ludwig Fund for Cancer Research (to C.L. Mackall), and a St Baldrick's/Stand Up 2 Cancer Pediatric Dream Team Translational Cancer Research Grant (to C.L. Mackall). Stand Up 2 Cancer is a program of the Entertainment Industry Foundation administered by the American Association for Cancer Research. C.L. Mackall is a member of the Parker Institute for Cancer Immunotherapy, which supports the Stanford University Cancer Immunotherapy Program.

The costs of publication of this article were defrayed in part by the payment of page charges. This article must therefore be hereby marked *advertisement* in accordance with 18 U.S.C. Section 1734 solely to indicate this fact.

Received July 16, 2020; revised September 23, 2020; accepted October 16, 2020; published first October 21, 2020.

References

1. June CH, Sadelain M. Chimeric antigen receptor therapy. N Engl J Med 2018;379:64–73.
2. Majzner RG, Mackall CL. Clinical lessons learned from the first leg of the CAR T cell journey. Nat Med 2019;25:1341–55.
3. Porter DL, Hwang W-T, Frey NV, Lacey SF, Shaw PA, Loren AW, et al. Chimeric antigen receptor T cells persist and induce sustained remissions in relapsed refractory chronic lymphocytic leukemia. Sci Transl Med 2015;7:303ra139.
4. Ali SA, Shi V, Maric I, Wang M, Stroncek DF, Rose JJ, et al. T cells expressing an anti-B-cell maturation antigen chimeric antigen receptor cause remissions of multiple myeloma. Blood 2016;128:1688–700.
5. Mueller KT, Maude SL, Porter DL, Frey N, Wood P, Han X, et al. Cellular kinetics of CTL019 in relapsed/refractory B-cell acute lymphoblastic leukemia and chronic lymphocytic leukemia. Blood 2017;130:2317–25.
6. Mueller KT, Waldron E, Grupp SA, Levine JE, Laetsch TW, Pulsipher MA, et al. Clinical pharmacology of tisagenlecleucel in B-cell acute lymphoblastic leukemia. Clin Cancer Res 2018;24:6175–84.
7. Awasthi R, Pacaud L, Waldron E, Tam CS, Jäger U, Borchmann P, et al. Tisagenlecleucel cellular kinetics, dose, and immunogenicity in relation to clinical factors in relapsed/refractory DLBCL. Blood Adv 2020;4:560–72.
8. Kochenderfer JN, Somerville RPT, Lu T, Yang JC, Sherry RM, Feldman SA, et al. Long-duration complete remissions of diffuse large B cell lymphoma after anti-CD19 chimeric antigen receptor T cell therapy. Mol Ther 2017;25:2245–53.
9. Maude SL, Laetsch TW, Buechner J, Rives S, Boyer M, Bittencourt H, et al. Tisagenlecleucel in children and young adults with B-cell lymphoblastic leukemia. N Engl J Med 2018;378:439–48.
10. Pule MA, Savoldo B, Myers GD, Rossig C, Russell HV, Dotti G, et al. Virus-specific T cells engineered to coexpress tumor-specific receptors: persistence and antitumor activity in individuals with neuroblastoma. Nat Med 2008;14:1264–70.
11. Keu KV, Witney TH, Yaghoubi S, Rosenberg J, Kurien A, Magnusson R, et al. Reporter gene imaging of targeted T cell immunotherapy in recurrent glioma. Sci Transl Med 2017;9:eaag2196.
12. Krebs S, Ahad A, Carter LM, Eyquem J, Brand C, Bell M, et al. Antibody with infinite affinity for *in vivo* tracking of genetically engineered lymphocytes. J Nucl Med 2018;59:1894–900.
13. Emami-Shahri N, Foster J, Kashani R, Gazinska P, Cook C, Sosabowski J, et al. Clinically compliant spatial and temporal imaging of chimeric antigen receptor T-cells. Nat Commun 2018;9:1081.
14. Minn I, Huss DJ, Ahn H-H, Chinn TM, Park A, Jones J, et al. Imaging CAR T cell therapy with PSMA-targeted positron emission tomography. Sci Adv 2019;5:eaaw5096.
15. Sellmyer MA, Richman SA, Lohith K, Hou C, Weng C-C, Mach RH, et al. Imaging CAR T cell trafficking with eDHFR as a PET reporter gene. Mol Ther 2020;28:42–51.
16. Chapelin F, Gao S, Okada H, Weber TG, Messer K, Ahrens ET. Fluorine-19 nuclear magnetic resonance of chimeric antigen receptor T cell biodistribution in murine cancer model. Sci Rep 2017;7:17748.
17. Weist MR, Starr R, Aguilar B, Chea J, Miles JK, Poku E, et al. PET of adoptively transferred chimeric antigen receptor T cells with 89Zr-oxine. J Nucl Med 2018;59:1531–7.
18. Lee SH, Soh H, Chung JH, Cho EH, Lee SJ, Ju J-M, et al. Feasibility of real-time in vivo 89Zr-DFO-labeled CAR T-cell trafficking using PET imaging. PLoS One 2020;15:e0223814.
19. Wei W, Rosenkrans ZT, Liu J, Huang G, Luo Q-Y, Cai W. ImmunoPET: concept, design, and applications. Chem Rev 2020;120:3787–851.
20. Beckford Vera DR, Smith CC, Bixby LM, Glatt DM, Dunn SS, Saito R, et al. Immuno-PET imaging of tumor-infiltrating lymphocytes using zirconium-89 radiolabeled anti-CD3 antibody in immune-competent mice bearing syngeneic tumors. PLoS One 2018;13:e0193832.
21. Pektor S, Schlöder J, Klasen B, Bausbacher N, Wagner D-C, Schreckenberger M, et al. Using immuno-PET imaging to monitor kinetics of T cell-mediated inflammation and treatment efficiency in a humanized mouse model for GvHD. Eur J Nucl Med Mol Imaging 2020;47:1314–25.
22. Freise AC, Zettlitz KA, Salazar FB, Lu X, Tavaré R, Wu AM. ImmunoPET imaging of murine CD4+ T cells using anti-CD4 cys-diabody: effects of protein dose on T cell function and imaging. Mol Imaging Biol 2017;19:599–609.
23. Freise AC, Zettlitz KA, Salazar FB, Tavaré R, Tsai W-TK, Hadjioannou A, et al. ImmunoPET in inflammatory bowel disease: imaging CD4+ T cells in a murine model of colitis. J Nucl Med 2018;59:980–5.
24. Mayer KE, Mall S, Yusufi N, Gosmann D, Steiger K, Russelli L, et al. T-cell functionality testing is highly relevant to developing novel immuno-tracers monitoring T cells in the context of immunotherapies and revealed CD7 as an attractive target. Theranostics 2018;8:6070–87.
25. Tavaré R, Escuin-Ordinas H, Mok S, McCracken MN, Zettlitz KA, Salazar FB, et al. An effective immuno-PET imaging method to monitor CD8-dependent responses to immunotherapy. Cancer Res 2016;76:73–82.
26. Seo JW, Tavaré R, Mahakian LM, Silvestrini MT, Tam S, Ingham ES, et al. CD8+ T-cell density imaging with 64Cu-labeled cys-diabody informs immunotherapy protocols. Clin Cancer Res 2018;24:4976–87.
27. Alam IS, Mayer AT, Sagiv-Barfi I, Wang K, Vermesh O, Czerwinski DK, et al. Imaging activated T cells predicts response to cancer vaccines. J Clin Invest 2018;128:2569–80.
28. Van Elssen CHMJ, Rashidian M, Vrbanac V, Wucherpfennig KW, Habre ZE, Sticht J, et al. Noninvasive imaging of human immune responses in a human xenograft model of graft-versus-host disease. J Nucl Med 2017;58:1003–8.
29. Xiao Z, Mayer AT, Nobashi TW, Gambhir SS. ICOS is an indicator of T cell-mediated response to cancer immunotherapy. Cancer Res 2020;80:3023–32.
30. Alam IS, Simonetta F, Scheller L, Mayer AT, Murty S, Vermesh O, et al. Visualization of activated T cells by OX40-immunoPET as a strategy for diagnosis of acute graft-versus-host-disease. Cancer Res 2020 Sep 8 [Epub ahead of print].
31. Greenwald RJ, Freeman GJ, Sharpe AH. The B7 family revisited. Annu Rev Immunol 2005;23:515–48.
32. Lynn RC, Weber EW, Sotillo E, Gennert D, Xu P, Good Z, et al. c-Jun overexpression in CAR T cells induces exhaustion resistance. Nature 2019;576:293–300.
33. Good Z, Spiegel JY, Sahaf B, Malipatlolla MB, Frank MJ, Baird J, et al. Identification of two CAR T-cell populations associated with complete response or progressive disease in adult lymphoma patients treated with Axi-Cel. Blood 2019;134:779.
34. Jena B, Maiti S, Huls H, Singh H, Lee DA, Champlin RE, et al. Chimeric antigen receptor (CAR)-specific monoclonal antibody to detect CD19-specific T cells in clinical trials. PLoS ONE 2013;8:e57838.
35. Beilhack A, Schulz S, Baker J, Beilhack GF, Wieland CB, Herman EI, et al. *In vivo* analyses of early events in acute graft-versus-host

Downloaded from http://aacrjournals.org/clincancerres/article-pdf/27/4/1058/2067888/1058.pdf by guest on 19 August 2022

disease reveal sequential infiltration of T-cell subsets. Blood 2005;106: 1113–22.
36. Kochenderfer JN, Yu Z, Frasheri D, Restifo NP, Rosenberg SA. Adoptive transfer of syngeneic T cells transduced with a chimeric antigen receptor that recognizes murine CD19 can eradicate lymphoma and normal B cells. Blood 2010;116: 3875–86.
37. Qin H, Ishii K, Nguyen S, Su PP, Burk CR, Kim B-H, et al. Murine pre-B-cell ALL induces T-cell dysfunction not fully reversed by introduction of a chimeric antigen receptor. Blood 2018;132:1899–910.
38. Zheng Z, Chinnasamy N, Morgan RA. Protein L: a novel reagent for the detection of chimeric antigen receptor (CAR) expression by flow cytometry. J Transl Med 2012;10:29.
39. Edinger M, Cao Y-A, Verneris MR, Bachmann MH, Contag CH, Negrin RS. Revealing lymphoma growth and the efficacy of immune cell therapies using *in vivo* bioluminescence imaging. Blood 2003;101:640–8.
40. Di Gialleonardo V, Signore A, Glaudemans AWJM, Dierckx RAJO, De Vries EFJ. N-(4-18F-fluorobenzoyl)interleukin-2 for PET of human-activated T lymphocytes. J Nucl Med 2012;53:679–86.
41. Kang L, Jiang D, England CG, Barnhart TE, Yu B, Rosenkrans ZT, et al. ImmunoPET imaging of CD38 in murine lymphoma models using 89Zr-labeled daratumumab. Eur J Nucl Med Mol Imaging 2018;45:1372–81.
42. Berger C, Flowers ME, Warren EH, Riddell SR. Analysis of transgene-specific immune responses that limit the in vivo persistence of adoptively transferred HSV-TK–modified donor T cells after allogeneic hematopoietic cell transplantation. Blood 2006;107:2294–302.
43. Freise AC, Wu AM. *In vivo* imaging with antibodies and engineered fragments. Mol Immunol 2015;67:142–52.
44. Fu R, Carroll L, Yahioglu G, Aboagye EO, Miller PW. Antibody fragment and affibody ImmunoPET imaging agents: radiolabelling strategies and applications. ChemMedChem 2018;13:2466–78.

Downloaded from http://aacrjournals.org/clincancerres/article-pdf/27/4/1058/2067888/1058.pdf by guest on 19 August 2022